

A GPU cluster optimized multigrid scheme for computing unsteady incompressible fluid flow

György Tegze*, Gyula I. Tóth

Institute for Solid State Physics and Optics, Wigner Research Centre for Physics P.O. Box 49, H-1525 Budapest, Hungary

Abstract

A multigrid scheme has been proposed that allows efficient implementation on modern CPUs, many integrated core devices (MICs), and graphics processing units (GPUs). It is shown that wide single instruction multiple data (SIMD) processing engines are used efficiently when a deep, 2h grid hierarchy is replaced with a two level scheme using 16h-32h restriction. The restriction length can be fitted to the SIMD width to fully utilize the capabilities of modern CPUs and GPUs. This way, optimal memory transfer is also ensured, since no strided memory access is required. The number of the expensive restriction steps is greatly reduced, and these are executed on bigger chunks of data that allows optimal caching strategies. A higher order interpolated stencil was developed to improve convergence rate via minimizing spurious interference between the coarse and the fine scale solutions. The method is demonstrated on solving the pressure equation for 2D incompressible fluid flow: The benchmark setups cover shear driven laminar flow in cavity, and direct numerical simulation (DNS) of a turbulent jet. We show that the scheme also allows efficient usage of distributed memory computer clusters via decreasing the number of memory transfers between host and compute devices, and among cluster nodes. The actual implementation uses a hybrid OpenCl/MPI based parallelization.

Keywords: interpolated stencil multigrid (ISM), additive correction multigrid (ACM), incompressible fluid flow, turbulence, computational fluid dynamics (CFD), direct numerical simulation (DNS)

1. Introduction

Numerical studies of incompressible fluid flow are important in both academic research and engineering applications. The incompressibility constraint and constant density represent a good approximation when fluid flow velocity is significantly smaller than the speed of sound in the media. For subsonic unsteady flows this approach usually allows larger time-steps, because, contrary to the compressible fluid models, density waves travelling at the speed of sound do not need to be resolved. However, solving for the pressure instead of density changes the continuity equation from parabolic to elliptic type. The major computational challenge in simulating incompressible unsteady fluid flow is to solve the elliptic pressure equation effectively in a parallel manner [1].

The demand for more detailed descriptions of convection phenomena, such as microscale description of multiphase systems, large eddy simulation (LES) or direct numerical simulation (DNS), drives evolution of mathematical and numerical tools along with the evolving computer architectures. Recently, the share of accelerator cards (i.e. GPUs), and multi-core coprocessors is rapidly

increasing in the supercomputing scene. Alongside, programming paradigms are changing to fully exploit the fine grained parallelism available on these hardwares. Writing GPU optimized codes for solving parabolic PDEs using explicit time marching is straightforward [2], while computationally efficient treatment of elliptic problems such as the Poisson equation used to force incompressibility requires more complex methods. The difficulty lies in the multilevel parallelism of the current supercomputing hardwares. While efficient methods exist to solve large scale elliptic problems on distributed memory hardware, it is not straightforward to optimize these algorithms for fine grain parallelism.

Multigrid (MG) methods are among the methods that are used to accelerate the iterative solution of large algebraic equations, such as those emerging from the discretizations of the pressure equation. The method decreases the number of iterations required to reach the convergence criteria via multi-resolution discretization that relaxes residuals on different wavelengths. The MG methods traditionally use a deep hierarchy of discretization, where each grid is 2h coarser than the previous level. The scheme development for this multi-resolution hierarchy needs special attention, since parallel execution of the iterations on fine meshes are usually bandwidth limited, while the solution of the coarser level discrete equations can be latency limited. Besides, it is difficult to achieve optimal

*Corresponding author, Tel: (+36) 1 392 2222 ext. 3839; Fax: (+36) 1 392 2219

Email address: turpi@tegze.net (György Tegze)

fine grain parallelism when using these schemes. Memory load performance, cache usage and SIMD utilization cannot be optimized at the same time, even if the programming model allows control over these procedures. The ease of programming is also an issue when evaluating a numerical procedure. While the MG methods are widely used in commercial programs, the complexity of the code prevents many scientist to implement such schemes in research codes. Not only field variables, but also boundary conditions must be consecutively transfered in the grid hierarchy in a way that ensures proper padding to keep data alignment. Compared to other programming languages, load balancing in streaming languages requires different approach, since it is not possible to launch and terminate "threads" inside compute kernels. Although the conventional 2h hierarchy of the multigrid scheme does not fit to streaming programming languages, it can be implemented on GPU architectures [3, 4].

Here a simple but effective two-level multigrid method is presented that bypasses most of the difficulties arising when implementing to many-core hardware architectures. The efficiency of the method will be demonstrated by solving the pressure equation for unsteady incompressible fluid flow. Simulation of a laminar flow in a shear driven cavity, and a direct numerical simulation of a turbulent jet have been used to benchmark our scheme.

2. The fluid model and its discretization

2.1. The equations of the incompressible fluid

Three assumptions on fluid behavior yields the Navier-Stokes equation: (i) The viscous dissipation is a linear function of the strain rates, (ii) the fluid is isotropic (rotational invariance), and (iii) for a fluid at rest hydrostatic pressure applies. Assuming incompressibility and constant density, the Navier-Stokes equation and the continuity of mass read as follows:

$$\frac{\partial \mathbf{v}}{\partial t} = \mathbf{v} \cdot (\nabla \otimes \mathbf{v}) + \eta \Delta \otimes \mathbf{v} + \nabla p \quad (1)$$

$$0 = -\nabla \cdot \mathbf{v} \quad (2)$$

where equation (1) is solved for the fluid velocity \mathbf{v} , and equation (2) is solved for the pressure p when substituting \mathbf{v} [see Eq. (4)]. η is the kinematic viscosity.

2.2. The time stepping scheme

Chorin's projection method [5] was chosen to solve the governing equations. We predict velocity \mathbf{v}^* for the next time-step using a simple first order time integration of the explicitly known terms. The pressure can be decomposed as: $p^{t+1} = p^t + \delta p$. Using p^t the predicted velocity reads as:

$$\mathbf{v}^* = \mathbf{v}^t + \Delta t [\mathbf{v}^t \cdot (\nabla \otimes \mathbf{v}^t) + \eta \Delta \otimes \mathbf{v}^t] + \nabla p^t. \quad (3)$$

Substituting $\mathbf{v}^{t+1} = \mathbf{v}^* + \nabla \delta p$ into Eq. (2) yields the following Poisson equation:

$$0 = \nabla \cdot \mathbf{v}^* + \nabla^2 \delta p, \quad (4)$$

which has to be solved for the pressure change δp . Finally \mathbf{v}^* is corrected with the pressure-change term $\nabla \delta p$ to obtain the divergence free \mathbf{v}^{t+1} .

2.3. The spatial discretization

A staggered grid arrangement [6] has been chosen for the velocity to avoid odd-even decoupling and the resulting spurious checkerboard patterns in the solution. Finite differences of second order accuracy were used to discretize the Navier-Stokes equation [7], and a five point Laplacian stencil was used to discretize the pressure equation. Alternatively, the discretization can be derived from finite volumes (FV) that gives a clear explanation of constructing flux preserving conservative stencils.

3. Solution of the continuity equation

While the explicit time marching scheme for the Navier-Stokes equation can be solved line by line, discretizing the continuity equation leads to a large system of linear equations. Direct solution of such systems is computationally too expensive for most practical problems, and also difficult to perform in a parallel manner. The discretization error is usually larger than the accuracy of the computer arithmetic, thus an approximate solution of the discrete problem is satisfactory, and an iterative solution can be applied. In parallel environment, the Gauss-Seidel (GS) iteration is commonly applied. Concurrent computing of the well known 5 point stencil is feasible when using red-black reordering [8], while multicolor ordering [9] can be used for higher order stencils.

3.1. Multigrid

The GS iterations are very effective in removing the high frequency components of the error, but the low frequency components decay with a very low rate. Convergence requires $O(N^2)$ iterations, where N is the linear size. Multigrid methods are commonly used to accelerate convergence: coarser discretizations are used to eliminate the lower frequency components of the residual. The MG technique consists of a sequence of smoothing, restriction, and prolongation operators. Smoothing steps are the actual iterations using a solver (i.e. Gauss-Seidel) on a grid level. Restriction is a downsampling the residual to a coarser discretization, and prolongation is an interpolation from a coarser to finer discretization. A typical multigrid cycle starts with smoothing of the residual error on the finest level, then the approximate solution is transfered to a coarser level (restriction), and smoothed again. The procedure is repeated until the coarsest level is reached,

then the way back. The optimal depth of the grid hierarchy depends on the actual problem, the discretized equations must be solved in a reasonable time on the coarsest level. A direct solver is often used at the coarsest grid.

When using a geometric multigrid (GMG) scheme, the original PDE is re-discretized on each grid, data structures must be constructed on each level. Note that the solutions on coarse grids does not necessarily approximate the solution on the fine grid, but it approximates the original problem. Possible inconsistency between fine and coarse grid solutions may results in extra iteration cycles before reaching convergence.

When using an algebraic multigrid (AMG) scheme, agglomeration of the coefficient matrix is performed. In the case of the widely used AMG procedure, the Additive Correction Multigrid (ACM) scheme [10], the coarse grid equations are obtained by the summation of the finer grid equations. The results obtained on the coarser grid are simply added to the finer grid solution, no interpolation or extrapolation operators are required in this procedure. The real advantage of this method is that on each level it approximates the solution of the discrete problem on the finest grid. Also note that conserving property of the spatial discretization scheme is satisfied at all discretization level. We extend the basic idea of the ACM scheme in our MG procedure.

It is often useful to interpret the discretization of the conservation equations (either momentum or mass) in the finite volume manner. When constructing a FV scheme, both sides of the PDE are integrated over a control volume (CV). Applying the Gauss theorem on the homogeneous part of the Poisson equation results in a surface integral of the fluxes over the CV faces. Thus simplest discretization is obtained, when the inhomogeneous part is assumed to be the CV average, and the surface normals of the pressure gradients are assumed to be constant at all CV faces. This recovers the well-known five point Laplacian stencil. The overall accuracy of the respective FV scheme depends both on the accuracy of calculating the fluxes on the CV face (using finite differences), and the accuracy of the surface integral [11].

After restricting the fine grid values to a coarser grid cell (hatched area in Fig. 1.), the same finite volume discretization procedure applies when the traditional geometric multigrid (GMG) method is used. However, one can use many values that are already pre-calculated on the fine mesh to make the discretization more accurate and easier to compute. For example, instead of downsampling \mathbf{v}^* to the coarse mesh and calculate its divergence using the corresponding finite volume stencil, one can sum $\nabla \mathbf{v}^*$ already calculated for the fine grid discretization. In the latter case the integration for the coarse CV will be the same accuracy as for the fine grid. The procedure is identical to the agglomeration of the coefficient matrix in the ACM method. Naturally, the integration (summation) can be applied for larger volumes too (a $8h$ restriction is shown in Fig. 1). Moreover one can perform similar sum for the fluxes de-

rived from applying the Gauss theorem for homogeneous part of the PDE. It is clear that fluxes not crossing the coarse grid cell faces cancel each other in the volumetric integral (summation), therefore, we have to account for the discretization only at the cell faces. When applying

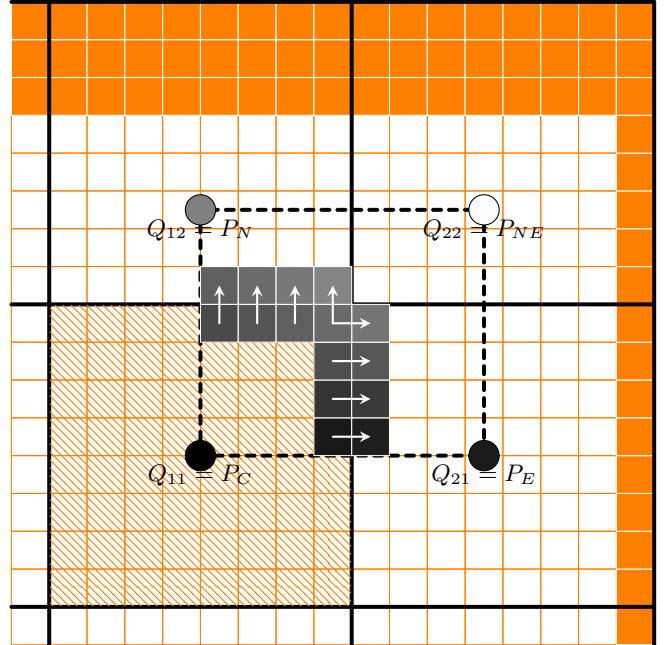


Figure 1: Multigrid layout: White rectangles show fine grid-cells, and orange coloring indicate padding to help coalesced read and write. Coarse grid is drawn by solid black lines, some cell centers (P_C, P_E, P_N and P_{NE}) are denoted with shaded circles. The actual center node for the coarse grid is hatched. The interpolation area for the north-east corner of the center node is indicated using dashed lines, and fine grid cells whose interpolated values used to construct the coarse grid discretized equations are shaded. White arrows show pressure gradients that are summed for the coarse grid discretization.

to domains of arbitrary size, an interpolation rule must be constructed to define fine grid pressure values $p_{i,j}$ near the boundaries. Thus the finite volume scheme for the coarse grid is constructed by summing fluxes calculated from the $p_{i,j}$ interpolated values. At this point the method differs from the ACM scheme, where a simple summation is performed that corresponds to assuming constant $p_{i,j}$ in the entire coarse CV. The neighboring coarse cells must use the same interpolated values to maintain the conservative character. This can be easily ensured, if these cells use a common domain to interpolate over. A natural choice is to interpolate between four neighboring cell centers (dashed rectangle in Fig. 1.). We have used a simple bilinear interpolation to calculate $p_{i,j}$ as a function of pressure values at the coarse cell centers $P_{i,j}$. Naturally, the same interpolation was used to prolongate the pressure values to the fine grid. If the origin is (Q_{11}) the bilinear interpolation reads as:

$$\begin{aligned}
p(x, y) = & \frac{1}{\Delta x^{W|E} \Delta y^{S|N}} [\\
& Q_{11}(\Delta x^{W|E} - x)(\Delta y^{S|N} - y) + \\
& Q_{21}x(\Delta y^{S|N} - y) + \\
& Q_{12}(\Delta x^{W|E} - x)y + \\
& Q_{22}xy],
\end{aligned} \tag{5}$$

where $\Delta x^{W|E}$ and $\Delta y^{S|N}$ are the horizontal, and the vertical size of the interpolation rectangle, while x and y are the coordinates of the fine grid control volume centers. The superscripts indicate that the size of the interpolation rectangle can differ on the west-east and the south north faces, because of padding, whereas the coarse mesh can be nonuniform. $Q_{I,J}$ are pressure values at the corners. Now, the fluxes across fine CV faces S_i and S_j (white arrows in Fig. 1.) can be computed as follows:

$$\begin{aligned}
\left. \frac{\partial p(x, y)}{\partial x} \right|_{S_j} = & \frac{1}{\Delta x^{W|E} \Delta y^{S|N}} [\\
& Q_{11}\{-1\}(\Delta y^{S|N} - y_j) + \\
& Q_{21}\{+1\}(\Delta y^{S|N} - y_j) + \\
& Q_{12}\{-1\}y_j + \\
& Q_{22}\{+1\}y_j]
\end{aligned} \tag{6}$$

and

$$\begin{aligned}
\left. \frac{\partial p(x, y)}{\partial y} \right|_{S_i} = & \frac{1}{\Delta x^{W|E} \Delta y^{S|N}} [\\
& Q_{11}\{-1\}(\Delta x^{W|E} - x_i) + \\
& Q_{21}\{-1\}x_i + \\
& Q_{12}\{+1\}(\Delta x^{W|E} - x_i) + \\
& Q_{22}\{+1\}x_i]
\end{aligned} \tag{7}$$

Summing up the above fluxes gives the discretization scheme for the coarse mesh. In practice the proper handling of the sum on the padded domain requires some integer arithmetics. Note that the above summation leads to a nine point stencil.

One can assume that not all discretization levels are equally important in reducing residual errors, thus the interpolated stencil with larger restriction steps can be applied. Fig. 2 shows a comparison of a common $2h$ V cycle and its two level "sparse" counterpart. Note that in the latter case, the number of restriction and prolongation steps are greatly reduced. In the next section we are going to investigate the effect of substituting common V cycles with sparse ones.

4. Implementation and benchmarking

All computations on the fine grid was implemented using the OpenCL streaming language. The language allows

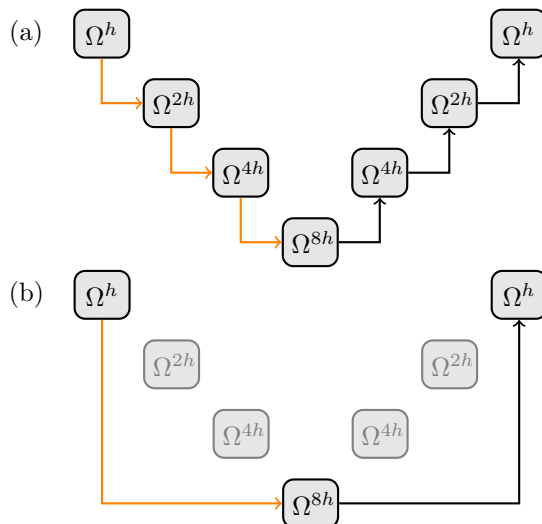


Figure 2: Schematic diagram of multigrid cycles: Ω^{xh} denote discretizations of different levels, orange, and black arrows correspond to restriction and prolongation steps, respectively. (a) V cycle using the conventional $2h$ restriction and prolongation steps. (b) sparse V cycle, when Ω^{2h} , and Ω^{4h} discretizations are bypassed.

an efficient use of SIMD engines via defining blocks of operations (work-groups) that are executed asynchronously. Work-groups can be either one, two or three-dimensional, thus explicit finite difference stencils are straightforward to implement; work-groups are paired with blocks of grided data (data "tiles" in 2D) [12]. In our software code each work-group corresponds to a coarse grid cell, thus code complexity is greatly reduced. The best computing efficiency can be achieved, when the tiles/work-groups are fitted to the SIMD width of the compute device.

Using optimal tile size on GPUs, the amount of data to be processed on coarse is greatly reduced (i.e., by a factor of 256 for a 16×16 tile size). In this case, it is likely that our iterations will be limited by the communication among cluster nodes. To avoid multiple load-store cycles, and network communication characterized by parallel multicolor iteration schemes [9], the serial Gauss-Seidel method is used on this grid level. The coarse grid solver was implemented as host code, using C language.

Code performance and our multigrid scheme was analyzed on various hardware platforms. We wish to emphasize that we have not put extra efforts in optimizing for specific platforms. Our aim was to measure the efficiency of the MG scheme on a more generic way, and give estimates on possible bottlenecks. We have not run the extra mile to prepare the whole scheme in native C, however some basic tests we have performed suggest that OpenCL gives at least a factor of two in efficiency, when compared to a "naive" C code using openMP parallelism.

4.1. OpenCl kernel performance

Our OpenCl compute kernel implementations use global memory, except reduction kernels (i.e. restrictions steps

in MG). This means that the kernels are quasi-optimal for CPUs, and further speedup is possible on graphics processors. The reason for using global memory access is its simplicity. We wanted to use exactly the same compute kernels on each platform, and we have not found a generic way to utilize the full potential of the specific hardware. Thus, our kernel timings can easily be achieved by a scientist or fluid dynamics expert, who is familiar with GPU programming at a basic level. Implementations of the finite difference stencils may also differ in flexibility of handling boundary conditions and grid size. Flexibility of the code often leads to conditional statements, which may dramatically affect code performance. In practice, conditional statements can mostly be replaced with integer, or bit-wise integer arithmetics, but leads to extra operations. We also note that architectures and platforms may significantly differ in performing integer operations that may result in differences in computing time for codes with flexible boundary conditions. Our kernel implementation uses automated padding if the grid size is not a multiple of the tile size, and can hold symmetric, Dirichlet and periodic boundary conditions. We use wall times of kernel execution as the measure of the performance. The results benchmarked on some recent hardware are summarized in Table 1.

Table 1: single chip kernel execution wall clock time/million grid points vs. work-group size

i5-2500K	4×4	8×8	16×16	32×32
Navier-Stokes	9.2 ms	10.1 ms	7.4 ms	7.9 ms
red-black GS	4.2 ms	3.3 ms	3.0 ms	3.2 ms
divergence	2.6 ms	1.7 ms	1.2 ms	1.2 ms
reduction	6.1 ms	7.8 ms	8.7 ms	12.4 ms
interpolation	8.8 ms	7.9 ms	7.7 ms	7.85 ms
GTX 680	4×4	8×8	16×16	32×32
Navier-Stokes	1.18 ms	0.68 ms	0.38 ms	0.39 ms
red-black GS	0.68 ms	0.22 ms	0.13 ms	0.15 ms
divergence	0.51 ms	0.20 ms	0.12 ms	0.13 ms
reduction	0.99 ms	0.30 ms	0.17 ms	0.27 ms
interpolation	1.06 ms	0.35 ms	0.33 ms	0.41 ms
Radeon 7970	4×4	8×8	16×16	32×32
Navier-Stokes	-	0.33 ms	0.28 ms	-
red-black GS	-	0.07 ms	0.06 ms	-
divergence	-	0.09 ms	0.06 ms	-
reduction	-	0.21 ms	0.12 ms	-
interpolation	-	0.31 ms	0.26 ms	-

According to the benchmarks, execution times are decreasing as work-group size increases on all hardware and saturates at the SIMD width. Its variation can be significant on GPUs. We note that with increasing restriction length we have double benefit; not just the computational cost of solving an iteration on the coarse mesh is decreasing, but also iterating on the fine grid becomes more efficient.

4.2. Multigrid performance

We have measured the computational cost of the MG scheme using the average number of computed Laplacians corresponding to a fine grid control volume in a time increment (N_{Lap}). This can be used to compare different MG schemes in an ideal case, where the network communication and the memory bandwidth are not limiting the calculation.

Although the computational cost of performing an iteration is an essential feature in evaluating a numerical method, the number of iterations required to reach convergence criteria is more fundamental, when evaluating scalability on large distributed memory computers. While the raw computational power can be increased by stacking computers, the interconnect latency and bandwidth have strict limitations. When performing finite difference iterations, the communication can be hidden up to the point, when compute time decreases to the network communication time. Down to this limit, the compute power can be fully utilized: theoretically the speedup is proportional to the number of processors. When pushing to this limit (i.e. by increasing the number of the compute devices), the total compute time can be reduced only via decreasing the iteration count, if we maintain computing efficiency. We use the total GS iteration count (I_t) and the related network communication count per time step (NCC_t) as the measure of performance on distributed memory clusters. We distinguish iteration numbers on fine (I_f) and coarse grids (I_c) since they behave differently with varying numerical parameters, and network communication characteristics also varies with grid size. The actual choice for the solver also influences network communication requirements: the simple GS involves 1 synchronization per iteration that doubles when red-black reordering is applied. Besides, when compute devices are external cards, an extra, compute device to host transfer is also involved.

4.2.1. benchmark setup I.: Shear driven laminar flow in cavity

In this section we use laminar flow in a rectangular cavity as a benchmark. The setup and the numerical parameters are shown in Fig.3. When using advanced multigrid methods, often complicated patterns are used to restrict and interpolate among various grid-levels, such as v-cycles and w-cycles. Here, the simplest accommodative cycles strategy is used: Iteration is started on the coarsest grid, and when the absolute maximum of the residual is decreased below a limit, the solution is interpolated to the finest grid. We can vary this criterion to find a quick solution. Then, iteration continues on the fine grid until reaching the fine grid convergence criterion. In our benchmark we require the residual to decrease below 10^{-6} on the fine grid, and vary the coarse grid criterion. Reaching this criterion requires significant efforts, but we are still comfortably far from the limits of the 32 bit float arithmetics.

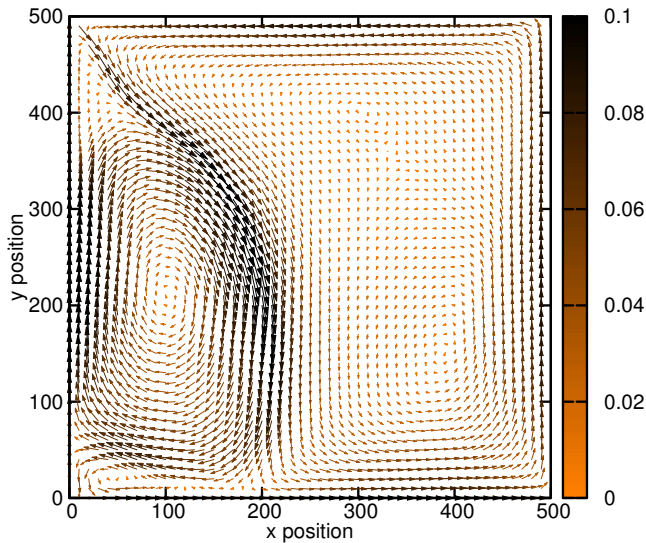


Figure 3: Benchmark I.: counter clockwise shear driven cavity flow with reversed velocity on the left, kinematic viscosity $\eta = 0.1$, velocity at the boundaries $v_0 = 0.1$, grid spacing $h = 1$, time-step $\Delta t = 1$ grid size 500×500 . Color code shows the magnitude of the velocity vectors.

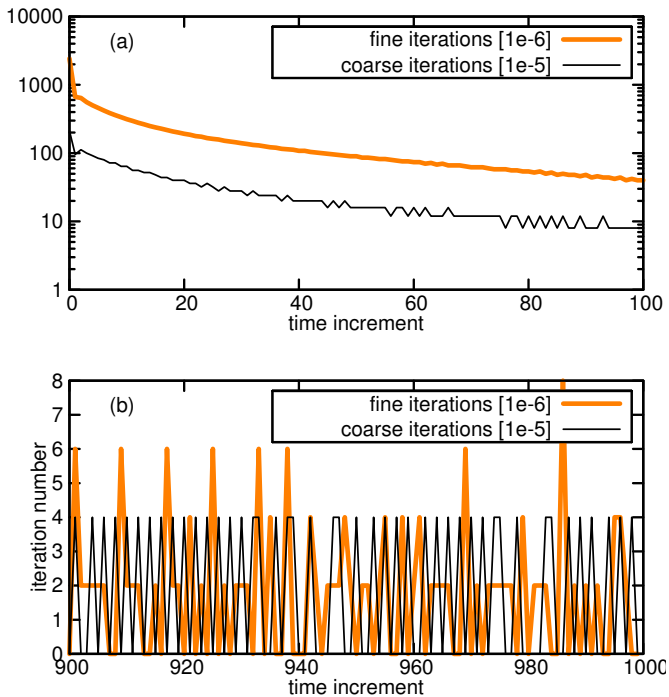


Figure 4: Benchmark I.: iteration numbers on the coarse and the fine grid vs. time increment. Convergence criteria was set to 10^{-6} and 10^{-5} for the fine and the coarse grid iterations, respectively. (a) very strong transient in first 100 time increments, (b) moderate transient between 900-1000 increments.

We have compared our results to the ACM scheme [13] that is using the conventional 2h restriction length. On the coarsest mesh, we have applied the same convergence

criterion as for the ISMG scheme. We have performed heuristic tests to find a quasi-optimal cycle: V cycles without pre-smoothing, and one post-smoothing per grid level was found to be a good candidate. The grid depth was varied, thus we have the ACM substitutes for our ISMG scheme using varying restriction length (e.g. tile size). In the case of our ACM implementation we denote only the coarsest mesh iterations as "coarse", and all the others are accounted as "fine". Iteration counts at each grid level can be calculated, since the number of the smoothing steps are the same, except for the coarse mesh.

We have measured scalability ($NCCs$) and computational cost (N_{Lap}) that are summarized in table A.2 for the ISMG scheme and in Table A.3 for the ACM scheme, respectively. The optimum values we have found are highlighted with bold characters. We have measured similar computational cost while our ISMG method requires six times less synchronizations. We note that the greatly reduced synchronization count also results in less kernel launches that is preferable in streaming computer languages. Besides, reduction and interpolation kernels are executed fewer times, however it is difficult to make a direct comparison on this basis, since it depends largely on the multigrid cycling pattern.

The low iteration counts we measured are partly due to the fact that in the ISMG scheme the coarse grid solution approximates the fine grid discrete solution. Fig. 4.b shows that in the moderate transient regime after interpolating to the fine grid the solution occasionally passing convergence criteria with no iterations. The same can be observed the way back, sometimes no coarse iteration is required after a converged solution of the previous time-step is applied in the predictor step.

4.2.2. benchmark setup II.: Turbulent jet

The previous test setup can be regarded as a synthetic benchmark, since the pressure we calculate is deterministic, therefore, one can tune the setup to provide unbiased benchmarks for the actual scheme (e.g. by varying the grid-size). In this section, we present benchmarks for Direct Numerical Simulation (DNS) of a turbulent jet. The actual setup, and the numerical parameters applied are shown in Fig. 5. Due to the chaotic nature of turbulence, it would be very difficult to tweak the test setup to show unbiased benchmarks, it can be accounted as a real-life application of our scheme. We have increased the grid size to 1000×2000 . Here we have maximized the number of GS iterations at 20000 for both ACM and ISMG computations to prevent convergence stagnation, however we believe this can be bypassed by using a more advanced cycling strategy. The linear sizes we have used in this setup are close to the supercomputing scale 3D direct numerical simulations.

Due to the increase in the linear size the small grid depth computations for ACM scheme and the corresponding 4×4 and 8×8 tile sizes in the ISMG scheme the solution is far from optimal and requires excessive compute

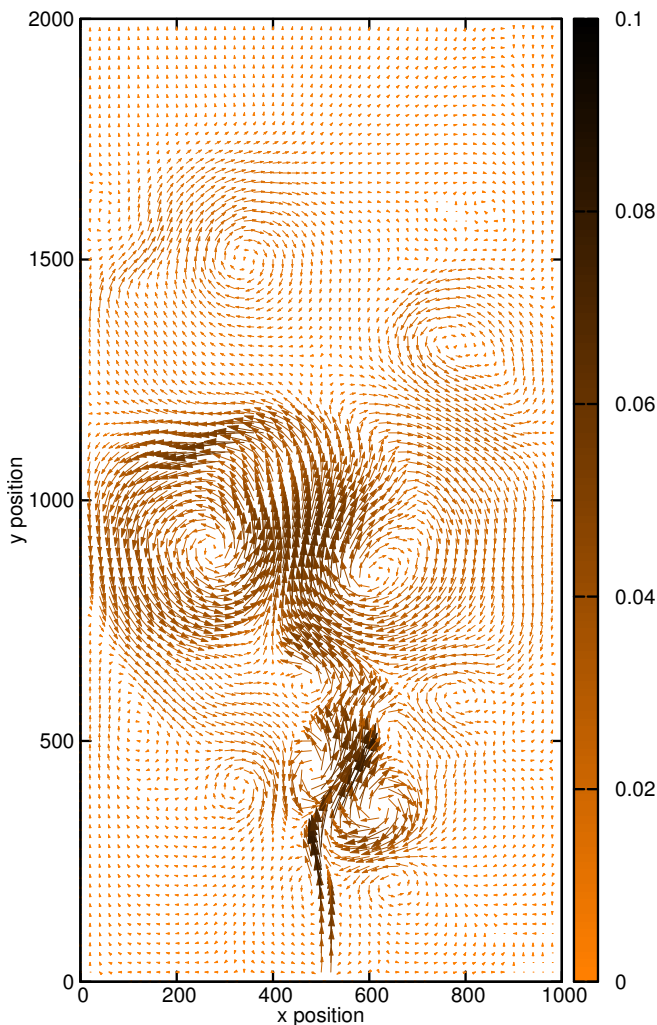


Figure 5: Benchmark II.: 2D turbulent jet flow in a rectangular cavity, no slip walls at the left and right boundaries; symmetry for velocity, and fixed pressure at the top boundary, and a tiny, 16 control volume wide inlet with $v_0 = 0.1$ is defined in the middle of the no slip bottom boundary, kinematic viscosity $\eta = 0.01$, grid spacing $h = 1$, time-step $\Delta t = 1$ grid size 1000×2000 . Color code shows the magnitude of the velocity vectors.

time, therefore results are not presented for these cases. The results for 5-6 grid levels of the ACM and the corresponding 16×16 and 32×32 tile size ISMG schemes are presented in Table A.4. In the case of the ACM scheme the optimum has been found at 6 grid levels contrary to the ISMG scheme, where the optimum has been found at 16×16 tile size (corresponds to 5 grid levels of the ACM method). Comparing the optima of the two methods, the ISMG scheme maintained the sixfold advantage in scalability (NCC_t), but at the cost of approximately twofold increase in the computational need (N_{Lap}). We note that in case of the applied cycling strategy this computational overhead is compensated by reduced restriction and interpolation counts, and their more efficient execution.

5. Concluding remarks

We have presented an interpolated stencil multigrid method that is efficient when 16-32h wide restriction step is applied. The stencil allows the replacement of a deep grid hierarchy (optimally 5-6 grid levels) with a two grid scheme, while keeping the number of iterations low. The scheme was benchmarked against an ACM scheme with deep grid hierarchy. It is shown that ISMG needs significantly less iterations compared to a conventional ACM scheme, since it involves less synchronizations (i.e. kernel calls and network communications). At larger grid sizes the raw computational cost (the number of the computed Laplacians) is increased by a factor of two, however it is overcompensated by the reduced number of interpolation and reduction kernel calls. Since in our current benchmarks we have used the simplest one-step accommodative cycling strategy, we are going to investigate more complex cycling patterns to further decrease computational cost. Using our method with higher order interpolation is also an issue that we wish to investigate. Since Gauss-Seidel has convergence rate of $O(N^2)$, where N is the linear size of the grid, the benchmarks presented in this paper can be used to give estimates for 3D cases. By extrapolating our benchmarks to 3D we expect that the ISMG method can be effective in supercomputing scale simulations with using a simple two grid scheme, or a three grid scheme using a direct solver on the third, coarsest level.

6. Acknowledgements

We thank L. Gránásy for illuminating discussions and for supporting our research. This work has been supported by the EU FP7 Collaborative Project EXOMET (contract no. NMP-LA-2012-280421, co-funded by ESA), and by the ESA MAP project GRADECET (Contract No. 4000104330/11/NL/KML). G. Tegze is a grantee of the János Bolyai Scholarship of the Hungarian Academy of Sciences.

Appendix A. Benchmarks

References

- [1] D. Kwak, C. Kiris, C. S. Kim, Computational challenges of viscous incompressible flows, *Computers and Fluids* 34 (3) (2005) 283–299. doi:10.1016/j.compfluid.2004.05.008.
- [2] P. Micikevicius, 3D finite difference computation on GPUs using CUDA, in: *Proceedings of 2nd Workshop on General Purpose Processing on Graphics Processing Units, GPGPU-2*, ACM, 2009, pp. 79–84. doi:10.1145/1513895.1513905.
- [3] J. Bolz, I. Farmer, E. Grinspun, P. Schröder, Sparse matrix solvers on the gpu: conjugate gradients and multigrid, *ACM Trans. Graph.* 22 (3) (2003) 917–924. doi:10.1145/882262.882364.
- [4] N. Bell, S. Dalton, L. Olson, Exposing fine-grained parallelism in algebraic multigrid methods, *SIAM Journal on Scientific Computing* 34 (4) (2012) C123–C152. doi:10.1137/110838844.
- [5] A. J. Chorin, Numerical solution of the navier-stokes equations, *Mathematics of Computation* 22 (1968) 745–762.

Table A.2: Benchmark I: the network communication counts in the fine ($LCSS_f$) and the coarse grid ($LCSS_c$), their sum ($LCSS_t$) and the raw computational cost (N_{Lap}) in the first 1000 time increment using the ISMG scheme for various tile sizes and coarse grid convergence criterion. Quasi optimal values are highlighted using bold characters.

tile size	4×4	8×8	16×16	32×32
<hr/>				
NCC_f	504^2	504^2	512^2	512^2
1×10^{-6}	5.0	9.7	21.4	50.8
1×10^{-5}	45.2	10.7	22.4	51.2
2×10^{-5}	166.1	13.4	23.8	51.6
3×10^{-5}	238.1	57.0	26.2	52.0
4×10^{-5}	262.2	78.3	28.9	52.6
5×10^{-5}	273.4	97.3	32.6	53.0
1×10^{-4}	296.9	221.0	85.4	59.5
<hr/>				
NCC_c	126^2	63^2	32^2	16^2
1×10^{-6}	72.8	47.4	31.2	17.4
1×10^{-5}	11.2	10.1	7.7	5.1
2×10^{-5}	4.3	6.5	5.2	3.8
3×10^{-5}	2.2	8.5	4.2	3.2
4×10^{-5}	1.5	2.5	3.6	2.9
5×10^{-5}	1.1	1.9	3.3	2.8
1×10^{-4}	0.5	0.6	3.1	2.3
<hr/>				
NCC_t				
1×10^{-6}	77.8	57.1	52.6	68.2
1×10^{-5}	56.4	20.8	30.0	56.3
2×10^{-5}	170.3	19.8	29.0	55.4
3×10^{-5}	240.2	65.5	30.4	55.3
4×10^{-5}	263.7	80.7	32.5	55.5
5×10^{-5}	274.6	99.2	35.9	55.8
1×10^{-4}	297.4	221.6	88.5	61.8
<hr/>				
N_{Lap}				
1×10^{-6}	7.0	5.6	10.8	25.4
1×10^{-5}	23.3	5.5	11.2	25.6
2×10^{-5}	83.3	6.8	11.9	25.8
3×10^{-5}	119.2	28.6	13.1	26.0
4×10^{-5}	131.2	39.2	14.5	26.3
5×10^{-5}	136.8	48.7	16.3	26.5
1×10^{-4}	148.5	110.5	42.7	29.8

Table A.3: Benchmark I: the network communication counts on the fine ($LCSS_f$) and the coarse grid ($LCSS_c$), their sum ($LCSS_t$) and the raw computational cost (N_{Lap}) in the first 1000 time increment using the ACM scheme for various grid-depths and coarse grid convergence criterion. Quasi optimal values are highlighted using bold characters.

grid depth	3 levels	4 levels	5 levels	6 levels
<hr/>				
NCC_f	256^2-	128^2-	64^2-	32^2-
1×10^{-6}	6.6	14.2	24.8	170.8
1×10^{-5}	48.2	15.0	25.4	170.8
2×10^{-5}	182.2	18.2	26.0	170.8
3×10^{-5}	259.8	51.2	27.2	170.8
4×10^{-5}	294.2	81.4	28.8	170.8
5×10^{-5}	314.0	115.4	30.8	170.8
1×10^{-4}	353.0	216.6	70.8	170.8
<hr/>				
NCC_c	128^2	64^2	32^2	16^2
1×10^{-6}	1012.0	1177.0	1151.4	0.0
1×10^{-5}	177.8	273.0	326.6	0.0
2×10^{-5}	77.4	165.8	211.2	0.0
3×10^{-5}	46.2	110.8	161.4	0.0
4×10^{-5}	33.0	81.4	132.4	0.0
5×10^{-5}	25.6	62.4	112.6	0.0
1×10^{-4}	11.8	26.2	57.2	0.0
<hr/>				
NCC_t				
1×10^{-6}	1018.6	1191.2	1176.2	170.8
1×10^{-5}	226.0	288.0	352.0	170.8
2×10^{-5}	259.6	184.0	237.4	170.8
3×10^{-5}	306.0	161.8	188.6	170.8
4×10^{-5}	327.2	162.8	161.0	170.8
5×10^{-5}	339.6	177.8	143.6	170.8
1×10^{-4}	364.8	242.8	128.0	170.8
<hr/>				
N_{Lap}				
1×10^{-6}	33.3	12.2	6.3	22.7
1×10^{-5}	17.6	5.3	4.8	22.7
2×10^{-5}	48.0	5.1	4.7	22.7
3×10^{-5}	66.4	11.5	4.8	22.7
4×10^{-5}	74.6	17.6	5.0	22.7
5×10^{-5}	79.3	24.5	5.3	22.7
1×10^{-4}	88.6	45.3	11.7	22.7

- [6] F. H. Harlow, J. E. Welsh, Numerical Calculation of Time-Dependent Viscous Incompressible Flow of Fluid with Free Surface, *The Physics of Fluids* 8, N. 10 (1965) 2182–2189.
- [7] W. E, J. guo Liu, A. I. E, Projection method iii: Spatial discretization on the staggered grid, *Math. Comp* 2001.
- [8] C. Kuo, T. Chan, Two-color fourier analysis of iterative algorithms for elliptic problems with red/black ordering, *SIAM Journal on Scientific and Statistical Computing* 11 (4) (1990) 767–793. doi:10.1137/0911045.
- [9] L. Adams, R. LeVeque, D. Young, Analysis of the sor iteration for the 9-point laplacian, *SIAM Journal on Numerical Analysis* 25 (5) (1988) 1156–1180. doi:10.1137/0725066.
- [10] B. R. Hutchinson, G. D. Raithby, A multigrid method based on the additive correction strategy, *Numerical Heat Transfer* 9 (5) (1986) 511–537. doi:10.1080/10407788608913491.
- [11] J. H. Ferziger, M. Peric, *Computational Methods for Fluid Dynamics*, Springer, Berlin, 1999.
- [12] P. Micikevicius, 3D finite difference computation on GPUs using CUDA, in: *Proceedings of 2nd Workshop on General Purpose Processing on Graphics Processing Units, GPGPU-2*, ACM, New York, NY, USA, 2009, pp. 79–84. doi:10.1145/1513895.1513905.
- [13] M. Guerrero, A. Oliva, U. P. de Catalunya. Departament de Màquines i Motors Tèrmics, Parallel multigrid algorithms for computational fluid dynamics and heat transfer[, *Universitat Politècnica de Catalunya*, 2000.

Table A.4: Benchmark II: the network communication counts the fine ($LCSS_f$) and the coarse grid ($LCSS_c$), their sum ($LCSS_t$) and the raw computational cost (N_{Lap}) in the first 100000 time increment using the ACM and ISMG schemes for various grid-depths/tile sizes and coarse grid convergence criteria. Quasi optimal values are highlighted using bold characters.

tile/depth	16×16	32×32	5 levels	6 levels
NCC_f				
1×10^{-6}	3.4	9.5	14.2	46.2
1×10^{-5}	3.5	8.6	4.4	138.8
2×10^{-5}	-	9.5	4.4	5.4
3×10^{-5}	-	8.1	4.4	5.4
4×10^{-5}	-	8.0	4.4	5.4
5×10^{-5}	-	8.7	4.6	5.4
1×10^{-4}	-	13.5	-	5.4
NCC_c				
1×10^{-6}	5.0	7.9	428.0	494.2
1×10^{-5}	755.4	4.1	184.0	269.2
2×10^{-5}	-	3.6	62.0	67.2
3×10^{-5}	-	2.7	198.8	121.0
4×10^{-5}	-	2.4	240.4	125.8
5×10^{-5}	-	2.5	272.8	104.4
1×10^{-4}	-	2.1	-	40.4
NCC_t				
1×10^{-6}	8.4	17.4	442.4	540.4
1×10^{-5}	758.9	12.8	188.2	408.0
2×10^{-5}	-	13.1	66.4	72.6
3×10^{-5}	-	10.7	203.0	126.4
4×10^{-5}	-	10.4	245.0	131.2
5×10^{-5}	-	11.2	277.2	109.8
1×10^{-4}	-	15.6	-	45.8
N_{Lap}				
1×10^{-6}	1.7	4.8	3.2	6.4
1×10^{-5}	4.7	4.3	1.1	18.6
2×10^{-5}	-	4.8	0.8	0.8
3×10^{-5}	-	4.1	1.1	0.8
4×10^{-5}	-	4.0	1.2	0.8
5×10^{-5}	-	4.4	1.3	0.8
1×10^{-4}	-	6.8	-	0.7